Developing and evaluating a hybrid wind instrument

Kurijn Buys[1)], David Sharp[1)], Robin Laney[1)]
[1)] Faculty of Science, Technology, Engineering and Mathematics, The Open University, Walton Hall, Milton Keynes, MK7 6AA, United Kingdom. David.Sharp@open.ac.uk

Summary

A hybrid wind instrument generates self-sustained sounds via a real-time interaction between a computed excitation model (such as the physical model of human lips interacting with a mouthpiece) and a real acoustic resonator. Attempts to produce a hybrid instrument have so far fallen short, in terms of both the accuracy and the variation in the sound produced. The principal reason for the failings of previous hybrid instruments is the actuator which, controlled by the excitation model, introduces a fluctuating component into the air flow injected into the resonator. In the present paper, the possibility of using a loudspeaker to supply the calculated excitation signal is evaluated. A theoretical study has facilitated the modelling of the loudspeaker-resonator system and the design of a feedback and feedforward filter to successfully compensate for the presence of the loudspeaker. The resulting self-sustained sounds are evaluated by a mapping of their sound descriptors to the input parameters of the physical model of the embouchure, both for sustained and attack sounds. Results are compared with simulations. The largely coherent functioning confirms the usefulness of the device in both musical and research contexts.

1 Introduction

Over the past few decades, numerous different electronic and digital musical applications have emerged and have been developed. One particular application, in the field of musical instrument design, involves the electronic extension of traditional musical instruments through electro-mechanical devices, to create so-called "augmented musical instruments".

An extensively studied example of instrument augmentation is the application of active control (initially used to suppress undesired sounds and vibrations) to musical instruments in order to alter their original functioning. For example, Guérard and Boutillon [1, 2] simulated an entire resonator while other works describe applications on both wind and string instruments [3, 4, 5]. A more advanced technique that is currently being investigated is "modal active control" which enables the adjustment of individual resonances of a resonator [6, 7].

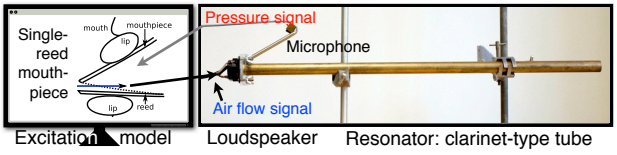

Figure 1: The hybrid wind instrument set-up: a computed mouthpiece in interaction with a physical resonator by means of a loudspeaker.

The concept laid out in the current paper concerns another class of augmented instruments, referred to as "hybrid instruments". In hybrid instruments, a crucial sound production component of the original instrument is replaced by an electronic equivalent. To date there has been relatively little research carried out on the concept of hybrid instruments. Weinreich and Caussé studied electronic excitation of a string, using both digital and analogue electronic interfaces [8]. Meanwhile, Maganza carried out a preliminary exploration of a set-up where a loudspeaker and microphone were used to enable an interaction between an "electronic excitation model" and a real acoustic resonator [9]. Since then several works on closely related subjects have been carried out, for example by Grand who used a custom-built electrovalve as a flow actuator [10]. Meanwhile, a more advanced electrovalve prototype was implemented by Buys and Vergez [11]. An important conclusion of these previous studies is that the actuator, which is the component that translates the computed flow rate output into a real acoustical flow, is critical to the accuracy of the operation of the hybrid instrument. More recently, Almeida extended the work of Maganza by adopting the same physical implementation, but with a linearised mouthpiece approach [12].

In the present study, the idea of using a loudspeaker to perform the actuation is continued. While the loudspeaker is not capable of generating a mean (DC) flow, that flow component is known to be of secondary importance for proper self-sustained functioning [13].

Figure 1 illustrates the concept of the hybrid instrument discussed in this paper. A physical model of a single-reed mouthpiece (including the player's mouth) is implemented on a computer and used as the "excitation model" to a real "clarinet-like" pipe (the resonator). This is achieved by measuring the pressure $p(t)$ at the resonator entrance with a microphone,

supplying it to the embouchure model and sending out the calculated flow-rate $q(t)$ via the loudspeaker. More generally, it is possible to introduce any excitation model; the model might be based on the physics of real components or it might be a purely theoretical design. As far as the acoustic resonator is concerned, the bore of any wind instrument with a near-to-closed entrance condition can be used.

Hybrid instruments support two main research interests. The first motivation, just like for all augmented musical instruments, is new musical potential, particularly in terms of timbre, which is an active musical composition focus of today. Here, the precise electronic control can play a role in the accessibility of certain (variations of) sounds. While the computed environment allows the modelling of any conceivable excitation and facilitates electronic parameter variations, the physical control over the resonator (the fingering) remains, which opens up an alternative range of musical expression with the advantage of relatively low computational power needs.

The second motivation lies in the context of acoustic wind instrument research. Specifically, it would be of substantial value to have a repeatable and precisely quantified control over an exciter that is linked to a resonator of interest. This matches with the objectives of the now well-established "artificial mouths" for wind instruments [14, 15]. Another concept is also of interest: studying how the excitation relates to the produced sound, by comparison with real and simulated wind instruments and with wind instrument theories such as described in [13].

The overall aim of the current work is to develop a stable practical implementation of a hybrid instrument, using a theoretical model of a single-reed mouthpiece as the excitation model in the first instance (although, as noted above, any excitation model could in principle be used).

To facilitate understanding of the theory underpinning the practical implementation of a hybrid instrument, in the next section a complete physical model of the clarinet is introduced. This complete model comprises a single-reed mouthpiece model and a resonator model in coupled interaction. In section 3, a proposed overall model for the hybrid instrument is briefly laid out. This model is expanded upon with some detailed theoretical discussion of how to compensate for the presence of the loudspeaker. Next, in section 4, the practical implementation of the hybrid wind instrument developed during this study is discussed. In section 5, the hybrid functionality is evaluated and compared with the simulations; and section 6 concludes and provides a brief discussion on the wider outcomes of the work.

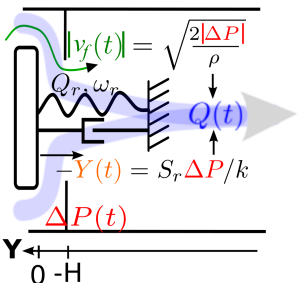

Figure 2: The single-reed mouthpiece model.

2 Physical model of clarinet

The acoustic operation of the clarinet can be understood as a bi-directional interaction between a nonlinear element — the mouthpiece — and a linear resonator, i.e. the acoustic duct. The following subsections provide descriptions of selected models of these components.

The convention used when presenting these models (and throughout the paper in general) is that time domain signals are denoted in lower case. Frequency domain signals, denoted in upper case, are expressed in the complex s-plane (for continuous time) by using the Laplace Transform with imaginary argument, with $s = j\omega$, $\omega = 2\pi f$ and f the frequency in Hz. Discrete spectra are expressed in the z-plane by applying the Z-transform with $z = e^{sT}$, with T the sample time. However, for simplicity the t, s and z function arguments are not repeated after the introduction of a variable.

2.1 Single-reed mouthpiece model

The classical single-reed mouthpiece model depicted in figure 2 has been adopted from Wilson and Beavers [14]. It was further developed by Hirschberg [13] and has become well-established as a useful simplified model of the single-reed excitation.

2.1.1 Reed displacement

The reed (including the player's lower lip) is considered to behave as a mass-spring-damper system, driven by the pressure difference across the reed $\Delta p = p_m - p$ (with $p_m(t)$ the mouth pressure and $p(t)$ the pressure inside the mouthpiece), acting on part of the reed surface S_r. Hence, the reed's dynamics are described by:

$$\frac{1}{\omega_r^2}\frac{d^2\,y}{dt^2} + \frac{1}{Q_r\,\omega_r}\frac{d\,y}{dt} + y = \frac{-S_r(p_m - p)}{k}, \qquad (1)$$

with $y(t)$, the displacement of the reed with stiffness k, resonance frequency ω_r and quality factor Q_r.

2.1.2 Entering flow rate

The air flow that enters the instrument can be expressed as the product of the flow velocity $v_f(t)$ and the effective reed opening area S_f. The former can be found by applying the Bernoulli theorem between the mouth and the reed flow channel (i.e. across the aforementioned pressure difference) while the latter is assumed to be linearly related to the reed displacement. The resulting flow rate can be expressed as:

$$q = \underbrace{\operatorname{sgn}(p_m - p)\sqrt{\frac{2|p_m - p|}{\rho}}}_{v_f} \underbrace{\mathcal{H}(y+H)(y+H)w}_{S_f}, \tag{2}$$

where ρ is the air density and w is the effective reed width. The sgn operator is introduced to make the calculation of negative flows possible and the Heaviside function $\mathcal{H}$ is included to ensure a zero flow rate when the reed hits the lay at position $y = -H$, which occurs above the "beating pressure" P_M.

These equations can be simplified and made dimensionless by defining $\bar{y} = \frac{y}{H}$, $\gamma = \frac{p_m}{P_M}$, $\bar{p} = \frac{p}{P_M}$ and $\bar{q} = \frac{q\,Z_c}{P_M}$ (where $Z_c = \frac{\rho c}{S_t}$ is the characteristic impedance of the resonator, with c the speed of sound and S_t the cross-sectional area of the tube):

$$\begin{cases} \dfrac{1}{\omega_r^2}\dfrac{d^2\,\bar{y}}{dt^2} + \dfrac{1}{Q_r\;\omega_r}\dfrac{d\,\bar{y}}{dt} + \bar{y} = \bar{p} - \gamma \\ \bar{q} = \operatorname{sgn}(\gamma - \bar{p})\sqrt{|\gamma - \bar{p}|}\zeta\mathcal{H}(\bar{y}+1)(\bar{y}+1), \end{cases} \tag{3}$$

where $\zeta(t)$ lumps all remaining embouchure parameters together and its time variation is related to the lip-pressure variation on the reed.

In these simplified equations, there are three significant independent parameters: P_M, which determines the signal amplitude (which, within the linear dynamic range of the resonator, doesn't affect the timbre of the sound), the mouth pressure γ and the mouthpiece parameter ζ, which both have an effect on the signal shape and attack, and thus the timbre of the sound [16].

It is assumed that the mouth pressure remains invariant in the presence of flow variations (i.e. the mouth is considered to be an ideal pressure source).

The discretisation of this model is further developed in appendix A.1.

2.2 Resonator

To a good approximation, the resonator of a clarinet can be assumed to be a linear system. Therefore a theoretical model based on a modal decomposition of the input impedance can be used. Moreover, for a tube of this type, with relatively widely spaced modes and with ends that approach the Neumann and Dirichlet conditions, each impedance peak can be described as a second order transfer function with real coefficients (see e.g. [17]). The impedance can thus be written as a sum of these transfer functions:

$$Z_t(s) = Z_c \sum_{n=1}^{N} \frac{a_n s}{\omega_n^2 + \frac{\omega_n}{Q_n}s + s^2}, \tag{4}$$

where $\{a_n, \omega_n, Q_n\}$ are the real modal coefficients (the amplitude, resonance frequency and quality factor of mode n). This technique allows for a good approximation of a finite number of N modes of the measured impedance.

It should be noted that the input impedance of the resonator is very low for mean flows, so it can be assumed that $Z_t(\omega = 0) \approx 0$ [13].

3 Hybrid instrument concept

3.1 General considerations

A hybrid instrument is constructed by implementing a theoretical embouchure model (such as the single-reed mouthpiece model described in section 2.1) on a real-time computing system, and putting it in interaction with a real resonator. To this end, a loudspeaker and a microphone, positioned at the entrance of the resonator, enable the conversion of an electrical signal to an acoustic signal and vice versa.

Providing that a reasonable quality microphone is chosen, its response can be assumed flat (i.e. the conversion can be assumed to be close to ideal, with the electrical signal produced being directly proportional to the acoustic pressure). However, this is not true for the loudspeaker; its dynamics cause the input-to-output response to be filtered. Therefore, in order to correct for this and create a flat frequency response, when constructing a hybrid instrument a preceding "inverse filter" must be placed before the loudspeaker.

In addition, the loudspeaker diaphragm doesn't present a rigid termination to the tube; it is in an acousto-mechanically coupled interaction with it. To compensate for the force on the diaphragm due to the pressure in front of it, a feedback controller must be incorporated into the hybrid instrument to instruct the voice coil to generate an opposite reaction force, making the membrane robust to external pressure variations.

Figure 3 shows a block diagram explaining the functioning of a hybrid instrument in terms of transfer functions. We will refer to this diagram throughout the remainder of the paper (to help with the signposting, the bracketed numbers on the diagram correspond to different subsections within the paper). For consistency, all signals and systems are expressed in the frequency domain (hence their notation in capital letters).

The "physical" part that makes up the lower half of the diagram contains the transfer functions of

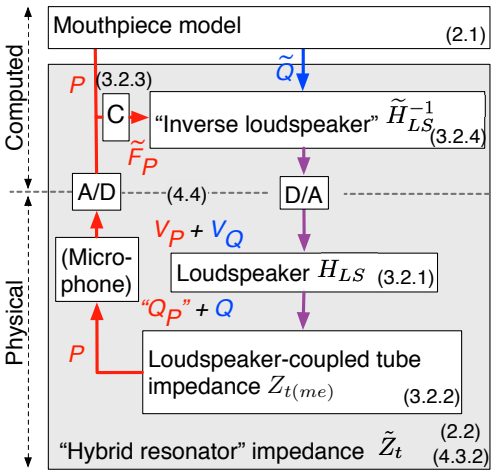

Figure 3: Block diagram of the hybrid instrument's computed and physical parts. The bracketed numbers correspond to different subsections within the paper.

the real physical components: the loudspeaker transfer function H_{LS} and the (loudspeaker-coupled) tube impedance $Z_{t(me)}$[1]. The "computed" part that comprises the upper half of the diagram contains two filters to cancel the loudspeaker's presence: a feedback controller C and a feedforward controller, represented by an "inverse loudspeaker transfer function" $\widetilde{H}_{LS}^{-1}$. The inclusion of a tilde sign for some of the transfer functions in the block diagram indicates that they are approximated versions of the associated transfer functions without a tilde. This also applies to some of the signals included in the block diagram.

The real-time computing system provides the interface between the "physical" part and the "computed" part. Its analogue-to-digital (A/D) and digital-to-analogue (D/A) converters are assumed to be free of any aliasing and quantization errors, while its total latency is assumed to be much smaller than the period of sounds generated by the hybrid instrument (see subsection 4.4). Provided this is the case, the computing system will provide a coherent approximation to the bi-directional interaction of the mouthpiece and resonator.

Stepping through the block diagram, the operation of the hybrid instrument is as follows. A computed flow rate signal $\widetilde{Q}$ (generated by the mouthpiece model) is sent to the "inverse loudspeaker" transfer function. The output is then sent through the D/A converter. This results in V_Q, a component of the total voltage signal that is provided to the loudspeaker.

[1]In the notation employed in this paper, the subscript can refer to the acoustic tube (by t) and the mechanical and electrical loudspeaker components (by respectively m and e). For coupled impedances, the leading symbol of the subscript indicates the type of impedance, while the subscripts entered between brackets indicate the elements it is coupled to. For instance, $Z_{t(me)}$ is an acoustic tube impedance for the case of a tube coupled to a loudspeaker, taking into account both the loudspeaker's mechanical and electrical components.

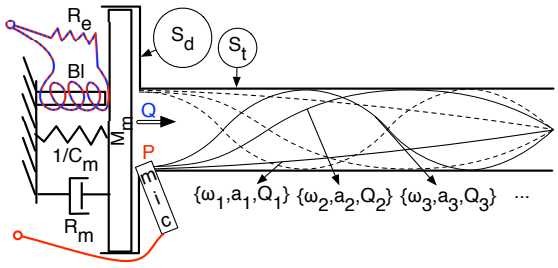

Figure 4: Schematic of the assembled loudspeaker and tube models. The variables R_e, Bl, C_m, R_m and M_m refer to loudspeaker parameters. S_d and S_t refer to respectively the loudspeaker diaphragm area and the tube cross-sectional area.

The latter, in response, generates a flow rate Q which is applied to the tube-resonator. In turn, the resonator reacts with a pressure P at its entrance. This pressure is captured by a microphone and acquired by the computer via the A/D converter. The feedback controller C uses this signal to generate a feedback force signal $\widetilde{F}_P$, which results in an additional voltage V_P provided to the loudspeaker. This component of the total voltage signal ensures that the signal produced by the loudspeaker compensates for the acoustical coupling with the tube (see subsection 3.2.3).

It should be noted that the coupling is interpreted in terms of an altered tube impedance, as this allows the impact on the original tube impedance to be studied. However, this is not a physically realistic representation (in reality the loudspeaker's response is affected by the coupling); hence the feedback flow rate Q_P is only a theoretical concept.

As the feedback filter compensates for the coupling, when combined with the coupled impedance $Z_{t(me)}$, an approximation of Z_t is obtained. Meanwhile, the feedforward filter $\widetilde{H}_{LS}^{-1}$ corrects for the loudspeaker response H_{LS}, so that all together an uncoupled (or, *hybrid*) tube impedance $\widetilde{Z}_t$ is obtained (represented by the large grey coloured frame in the block diagram). This impedance can also be understood in terms of the ratio of the measured pressure over the calculated flow rate. It is then available for interaction with the mouthpiece model so that hybrid self-sustained sounds can be produced.

3.2 Theoretical development

This section provides detailed theoretical descriptions of the loudspeaker, its interaction with the resonator in the form of a coupled system (as represented in figure 4) and the design of filters to compensate for the loudspeaker. The discussions are spread over four subsections, which also relate to the components of the block diagram in figure 3.

In the theoretical development, the sound is assumed to propagate in the form of plane waves, which is valid as long as the wavelength is much greater than the cross-sectional diameter of the tube and loud-

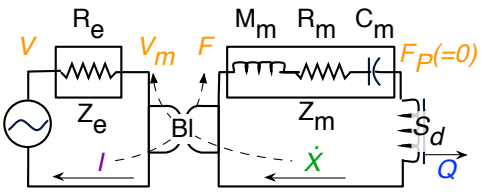

Figure 5: Equivalent electronic circuit representing the loudspeaker's electronic part (the impedance Z_e on the left, consisting of a resistive component R_e) and its mechanical part (the impedance Z_m on the right, consisting of inertia M_m, resistive R_m and compliance C_m components).

speaker [13]. Also, provided that the volume between the loudspeaker diaphragm and the tube is small, the change in cross-sectional area between the loudspeaker (with diaphragm area S_d) and the tube (with area S_t) is assumed to have negligible influence on both the flow rate Q and the pressure P, so that they can be considered as equal in and between both places.

3.2.1 Loudspeaker

To be able to employ a loudspeaker as the "flow generating" device in a hybrid instrument, it is important to have a detailed understanding of its behaviour in terms of its input-to-output response.

We adopt the classical linear (small-signal) model that was initially proposed by Small [18]. To aid understanding, and as typically used in loudspeaker theory [19] (and also often in mechanics and acoustics [20]), this model can be represented using the analogous electronic circuit theory to obtain an equivalent circuit as depicted in figure 5.

The equivalent circuit includes an electrical part with $Z_e = R_e$, the DC resistance of the voice coil, with voltage $V(s)$ at the input (the voice coil inductance is not taken into account here, as it is of negligible importance in our study), producing a current $I(s)$. It also includes a mechanical part which is modelled by a 1-DOF mass-spring-damper system (with the Thiele/Small electromechanical parameters M_m, C_m and R_m respectively the mass, inverse spring stiffness and damping coefficient), and receives a force $F(s) = Bl\ I$ from the voice-coil (with Bl, the voice-coil's "force factor"). This results in a membrane velocity $\dot{X}(s)$, which induces a feedback voltage $V_m(s) = Bl\ \dot{X}$ over the coil.

It has been shown that the electrical coupling only has a significant effect on the Q- (quality) factor of the mechanical impedance [18], so that:

$$Z_{m(e)}(s) = \frac{F_e}{\dot{X}} \approx \frac{M_m(\omega_{LS}^2 + \frac{\omega_{LS}}{Q_{ts}}\ s + s^2)}{s}, \qquad (5)$$

where $F_e = F + Bl\ V_m/Z_e = Bl\ V/Z_e$ is a virtual force, $\omega_{LS} = \sqrt{M_m^{-1}\ C_m^{-1}}$ is the speaker's resonance frequency, $Q_{ts} = \frac{\sqrt{M_m/C_m}}{R_{ts}(R_m,R_e)}$ is the coupled or "total" Q-factor and R_{ts} the total damping coefficient.

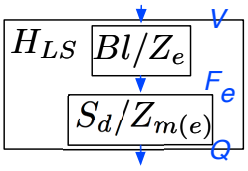

Figure 6: Block diagram of the loudspeaker's transfer function H_{LS}, consisting of the electrical part Bl/Z_e and the (electrical-coupled) mechanical part $S_d/Z_{m(e)}$.

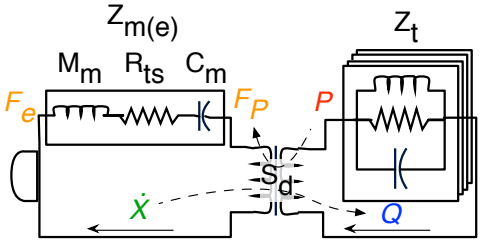

Figure 7: Equivalent electronic circuit representing the loudspeaker's mechanical part (including its coupling with the electronic part) coupled with the modal tube impedance.

Using Kirchhoff's circuit laws, the transformer relationships and equation (5), the complete loudspeaker system can then be represented by an overall transfer function that expresses the volume flow rate per input voltage:

$$H_{LS}(s) = \frac{Q(s)}{V(s)} = \frac{Bl}{Z_e}\frac{S_d}{Z_{m(e)}}, \qquad (6)$$

where $Q(s) = S_d\ \dot{X}$ is the volume flow rate generated by the loudspeaker.

The total loudspeaker transfer function as represented in the block diagram in figure 3 can thus be decomposed into Bl/Z_e and $S_d/Z_{m(e)}$ (see figure 6).

3.2.2 Coupling of loudspeaker and resonator

When mounting the loudspeaker on a tube, a coupled system is formed. The resonances of the coupled system are based on those of the loudspeaker and the tube, but are altered in frequency and amplitude, particularly where the loudspeaker and tube resonance frequencies lie close to each other. In this subsection we investigate how this coupling can be modelled, which will contribute to the choice of suitable components for a practical implementation of a hybrid instrument.

To model a loudspeaker that is coupled to a tube, we can simply combine the analogous loudspeaker circuit of figure 5 with an analogous circuit for the tube based on the modal decomposition of the input impedance (see section 2.2), which results in the circuit represented in figure 7. Note that this figure uses the simplified representation of the loudspeaker mechanics (see equation (5)).

Following the analogy of voltage representing pressure, the coupling between the loudspeaker and the tube is represented by a transformer, relating the force $F_P(s)$ and velocity $\dot{X}(s)$ of the loudspeaker membrane respectively to the pressure $P(s)$ and the flow rate $Q(s)$ at the instrument entrance by: $F_P = S_d\ P$ and $\dot{X}\ S_d = Q$. Hence, the loudspeaker-coupled tube impedance represented by this parallel circuit can be calculated by:

$$Z_{t(me)}(s) = \left(\frac{1}{Z_t} + \frac{S_d^2}{Z_{m(e)}} \right)^{-1}, \tag{7}$$

which is represented in the global block diagram in figure 3.

Considering equations (7), (5) and (4) for a single mode n, a "coupling frequency" can be defined as $\omega_{cn} = \sqrt{\frac{Z_c S_d^2 a_n}{M_m}}$.

For the case where the loudspeaker resonance frequency is far below the tube resonances, it can be shown that the larger the coupling frequency, the greater the shift in both the resonance frequency and the Q-factor of the mode.

Hence, given that the coupling frequency ω_{cn} is proportional to the the diaphragm area S_d and inversely proportional to the square root of M_m, it can be concluded that, for a real hybrid instrument, the choice of a small diaphragm loudspeaker with a heavy membrane would ensure a low coupling with the tube, which is a desirable initial situation. This is important because, as will be formulated in the next subsection, even though the coupling can be compensated for by electronic means, the size of the deviations caused by approximation errors in the real system will be higher the more the initial coupled system differs from the targeted "uncoupled" system.

In a similar manner, it can be shown that for the case where the loudspeaker resonance frequency is close to or above the first tube resonance, there is a high risk of a strong coupling with one of the tube modes. This situation should therefore be avoided.

Later, the coupled loudspeaker-tube model will be used to obtain the loudspeaker parameters with measured data (see appendix B). In order to derive useful expressions that are compatible with those measurements, the coupling can also be interpreted as an altered electrical loudspeaker input impedance, which can be obtained from the signals in the circuit in figure 5:

$$Z_{e(mt)}(s) = \frac{V}{I} = \frac{Z_e\ V}{V - V_m} = \frac{Z_e\ V}{V - Bl\ \dot{X}}. \tag{8}$$

Similarly, considering both circuits in figures 5 and 7, the coupled mechanical impedance can be written as:

$$\begin{aligned} Z_{m(et)}(s) &= Z_{m(e)} + S_d^2\ Z_t = Z_{m(e)} + S_d\ \frac{P}{\dot{X}} \\ &= \frac{F_e - F_P}{\dot{X}} + S_d\ \frac{P}{\dot{X}} = \frac{F_e}{\dot{X}} = \frac{V\ Bl}{Z_e\ \dot{X}}. \end{aligned} \tag{9}$$

3.2.3 Compensating for loudspeaker-tube coupling

As mentioned earlier, the principle behind the feedback filter that compensates for the coupling between the loudspeaker and tube is very simple: in order to undo the force on the loudspeaker diaphragm due to the pressure in front of it ($F_P = S_d\ P$), it is necessary to generate an opposite force with the voice coil. As P is directly measured by the microphone and the voice coil force can be obtained by using $\frac{Z_e}{Bl}$, the ideal feedback controller is simply:

$$C(s) = -S_d. \tag{10}$$

This expression is valid provided that the computing system's latency is small compared with the period of the waves to be controlled (see subsection 4.4).

The implementation of the control loop is depicted in the block diagram in figures 3 and 8.

3.2.4 Correcting for loudspeaker response

If the loudspeaker is not coupled with the tube (corresponding to the situation after successful application of the feedback filter), the feedforward filter to undo the loudspeaker's response is simply the inverse of its transfer function (6):

$$H_{LS}^{-1}(s) = \frac{Z_e}{Bl} \frac{Z_{m(e)}}{S_d}. \tag{11}$$

While the inverse of the electronic part of the loudspeaker's transfer function is simply $\frac{Z_e}{Bl} = \frac{R_e}{Bl}$, the mechanical part is not that easy to correct for and there are several reasons to opt for a loudspeaker that has a resonance frequency much lower than the tube resonance frequencies.

One reason is that the response around the loudspeaker's resonance frequency can be nonlinear in practice. Another reason, as demonstrated earlier for the situation where the loudspeaker is coupled to the tube, is that a heavier membrane minimises the coupling. Finally, this choice enables an inverse filter to be used, which also has the additional advantage of allowing the mean flow component to be removed from the signal sent to the loudspeaker.

This inverse filter can be derived in two steps. First, by considering eq. (5), at high frequencies the impedance approaches the inertia term, which is a pure derivative:

$$Z_{m(e)} \approx M_m\ s,\ (\text{if } s \gg j\omega_{LS}). \tag{12}$$

Then, given that the influence of the damping and the stiffness increases both the amplitude and phase at frequencies closer to the loudspeaker resonance, the addition of a filter H_{LL}, known as a "lead-lag compensator" (a filter to improve an undesirable frequency

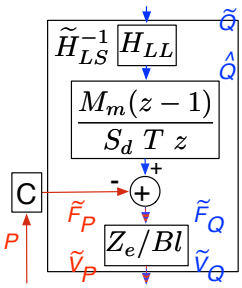

Figure 8: Block diagram of the transfer functions of the feedback filter C and the feedforward filter $\widetilde{H}_{LS}^{-1}$, consisting of the electrical part Z_e/Bl, the approximated (electrical-coupled) mechanical part $M_m(z-1)/(S_dTz)$ and the lead-lag filter H_{LL}.

response in a feedback system) can compensate for this effect down to $s = 2\,j\omega_{LS}$, so that:

$$Z_{m(e)} \approx H_{LL}\ M_m\ s,\ \text{(if } s \geq 2\,j\omega_{LS}\text{)}. \tag{13}$$

A desirable lead-lag filter response can be obtained using a biquadratic second order transfer function with complex poles and zeros [21]:

$$H_{LL} = \frac{s^2 + \frac{\omega_{LLn}}{Q_{LL}} s + \omega_{LLn}^2}{s^2 + \frac{\omega_{LLd}}{Q_{LL}} s + \omega_{LLd}^2}, \tag{14}$$

which provides the unique combination of zeros that decrease the amplitude and phase responses towards ω_{LS}, while the poles (situated at lower frequency) reset the gain from increasing to constant in the sub-ω_{LS} zone (and as such the removal of the mean-flow component is maintained). The numerator and denominator are modelled with resonance frequencies ω_{LLn} and ω_{LLd} and they share a common quality factor Q_{LL}, which is a convenient parametrisation that guarantees a converging curve regression to find optimal parameter values.

The discretisation of this filter is further developed in appendix A.2. Hence, taking into account equations (19) and (20), the feedforward filter's transfer function, as represented in the block diagram in figure 3, can be written as:

$$\widetilde{H}_{LS}^{-1}(z) = H_{LL} \frac{M_m\ (z-1)}{S_d\ T\ z} \frac{Z_e}{Bl}, \tag{15}$$

and its composition is depicted in figure 8.

4 Design of hybrid set-up

Section 3 discussed a theoretical framework for a real hybrid instrument. In this section, the practical implementation of a prototype hybrid instrument is described. This prototype has been built to enable the hybrid wind principle to be studied in practice.

First, the different components of the prototype instrument are introduced, including a discussion on the choice of loudspeaker. Then measurements designed to characterise the system are presented.

4.1 Resonator and associated hardware

For the resonator of the prototype hybrid instrument, a cylindrical tube has been chosen with dimensions (length 58 cm, inner diameter 14.2 mm) that approximately match those of a soprano clarinet playing its lowest note.

A Cambridge Audio type A1 power amplifier and a B&K microphone type 4135 are used. The microphone is mounted at the entrance of the resonator, just in front of the loudspeaker diaphragm. The responses of the amplifier and the microphone can be considered flat for the purpose of this study, as their gain and phase are found to deviate by less than ± 0.42 dBV and ± 0.1 rad respectively, in a frequency band far exceeding the hybrid operation. These deviations are much smaller than those that can be expected from the loudspeaker's response.

4.2 Choice of optimal loudspeaker

There are various criteria when it comes to identifying a loudspeaker suitable for use in a hybrid instrument.

Considering the previously discussed theoretical models, $\widetilde{H}_{LS}^{-1}$ tends towards H_{LS}^{-1} when ω_{LS} is much lower than the tube resonance frequencies. However, it should be noted that this scenario usually corresponds to a loudspeaker with a larger diaphragm or, by adding mass to the diaphragm, a reduction of the acoustic power, i.e. the sensitivity of the loudspeaker.

While the theory presented in section 3.2 implies that, for any given loudspeaker, the loudspeaker-tube coupling can be undone by the feedback loop, there are reasons to opt for a weak physical coupling. If one considers an erroneous signal P_{err} that accompanies the pressure measurement, it will be manifested as a false surplus flow rate $Q_{err} \approx P_{err}\ \frac{S_d^2}{M_m\ s}$, which indicates that light and especially large diaphragms are a likely source of instability in practice.

Another reason for choosing S_d to be small, is that the inevitable additional acoustic volume between the diaphragm and the tube entrance will be smaller. In this way the total entrance impedance is closer to the independent tube impedance and the "plane wave assumption" is valid to higher frequencies.

That said, the dynamic range of the system is determined by the power rating of the loudspeaker. More precisely, it is the RMS current through the loudspeaker coil that roughly indicates its temperature and therefore its maximum rating [22] (the maximum diaphragm excursion also can be of importance at low frequencies). As the flow rate related signal and the signal related to the feedback filter produce electrical currents in the coil, they should both be taken into account when estimating the electrical power. Whereas the former is inversely related to S_d (specifically $I_{\widetilde{Q}} \approx \widetilde{Q}\ \frac{M_m\ s}{S_d\ Bl}$), the latter is proportional to

S_d (specifically $I_P \approx P\ \frac{S_d}{Bl}$) and does not depend on the frequency. For optimal efficiency, these currents should be minimised by considering the loudspeaker parameters. However, this is not a straightforward procedure, as the correlation between the flow rate and pressure signals depends on the tube losses and the applied excitation model. An approximation can be obtained by stating that generally for wind instruments $|\ Q\ Z_c\ | \approx | \zeta\ P\ |$, with $0.1 \lesssim \zeta \lesssim 0.4$ [16].

Given that there is no straightforward mathematical relationship between the loudspeaker properties of interest (the membrane size and mass, the general frequency response, the power rating and the sensitivity), it can be concluded that there is no systematic means of finding the most suitable loudspeaker. However, it is possible to obtain good indications for the choice by following the theoretically determined guidelines.

Interestingly, it seems that the most suitable configuration of loudspeaker is not available as an off-the-shelf product, as its design is not appropriate for a standard audio application. For instance, it would be desirable in our context to have a small-diaphragm loudspeaker (usually only available as low-power units) with a thick-wire voice-coil, to enable high power ratings. Although the heavy coil would decrease the loudspeaker's sensitivity, it would ensure that the loudspeaker's resonance frequency remains much lower than the tube resonance frequencies.

For the prototype hybrid wind instrument, therefore, the idea of adding mass to a commercially available loudspeaker was explored. By applying the theoretical guidelines, a 1" Tang Band W1-1070SE loudspeaker was chosen. The datasheet specifies a large frequency bandwidth and a resonance frequency of $f_{LS} = 170\,\mathrm{Hz}$ that, by attaching a mass of 8.1 g to the membrane, was lowered to half the value of the first tube resonance frequency. This modified loudspeaker is hermetically mounted on the resonator by means of an adaptor. While still allowing for the loudspeaker diaphragm's full range of movement, this adaptor is designed as small as possible in order to minimise the additional volume, and thus its effect on the resonator impedance.

When this loudspeaker is coupled to the tube, the coupling frequency is $\omega_{c1} = 2\pi{\times}73.6\,\mathrm{rad\,s^{-1}}$. This results in a shift in the first tube resonance frequency from $2\pi{\times}139.7\,\mathrm{rad\,s^{-1}}$ to $2\pi{\times}157.8\,\mathrm{rad\,s^{-1}}$, with the Q-factor reduced by a factor of 0.33.

(It is worth noting that the frequency shift would be much larger for a loudspeaker with a greater $\frac{S_d^2}{M_m}$ factor, coupled to the same tube. Also, for a loudspeaker with a 2" diaphragm, the reduction in Q-factor would be ten times greater. This illustrates and explains the choice of a loudspeaker with a 1" diaphragm.)

Considering the power efficiency of this loudspeaker, with a close to sinusoidal self-sustained operation (so with $\zeta \approx 0.1$) at 140 Hz, we find $|I_{\widetilde{Q}}| = \{1.13\ 10^{-2} \times |P|\}\mathrm{A}$ and $|I_P| = \{2.39\ 10^{-2} \times |P|\}\mathrm{A}$. These are of the same order and thus result in a good power efficiency (as other S_d values result in an increase of either $I_{\widetilde{Q}}$ or I_P). Nevertheless, it should be borne in mind that additional harmonics and/or playing of higher pitched notes would rapidly increase $|I_{\widetilde{Q}}|$, such that a greater S_d would be more convenient in this regard.

Table 1: The estimated loudspeaker and H_{LL} parameters.

R_s	$6.32\,\Omega$	S_d	$6.95 \times 10^{-4}\,\mathrm{m^2}$
R_e	$6.08\,\Omega$	ω_{LS}	$2\pi{\times}67.4\,\mathrm{rad\,s^{-1}}$
Bl	$3.08\,\mathrm{T\,m}$	M_m	$8.52 \times 10^{-3}\,\mathrm{kg}$
Q_{ts}	1.48	ω_{LLn}	$2\pi{\times}82.9\,\mathrm{rad\,s^{-1}}$
Q_{LL}	1.73	ω_{LLd}	$2\pi{\times}46.2\,\mathrm{rad\,s^{-1}}$

4.3 Loudspeaker and tube characteristics

4.3.1 Parameter identification

To obtain all parameters of the coupled loudspeaker-tube system at the heart of the prototype hybrid instrument, a protocol involving two measurements and four least square linear regressions was applied. The details can be found in appendix B and the resulting loudspeaker and lead-lag filter parameters are presented in table 1.

4.3.2 Comparing measured and theoretical impedances

In order to establish how well the filters compensate for the loudspeaker, the impedance $\widetilde{Z}_t^* = P^*/\widetilde{Q}^*$ (the asterisks refer to measured quantities) can be compared with the measured tube input impedance $Z_t^* = P^*/Q^*$ (obtained in appendix B). Ideally, these two impedances should match, but there are several theoretical and practical approximations that may prevent them from doing so. To study the impact of particular approximations, it is useful to consider the transition between intermediate states of the impedance, where only a few approximations at a time are taken into account.

The focus of the comparison can be narrowed further. As the intended application of the hybrid wind instrument is the production of self-sustained sounds, the principal frequency components are harmonics that lie close to the positive impedance peaks of the resonator's input impedance. Moreover, given that only the first few modes are of importance to maintain the self-sustained operation, the amplitude and phase of only the first five modes are studied.

Following this approach, the measured tube impedance Z_t^* is depicted in figure 9 (in solid green) along with the loudspeaker-coupled tube impedance

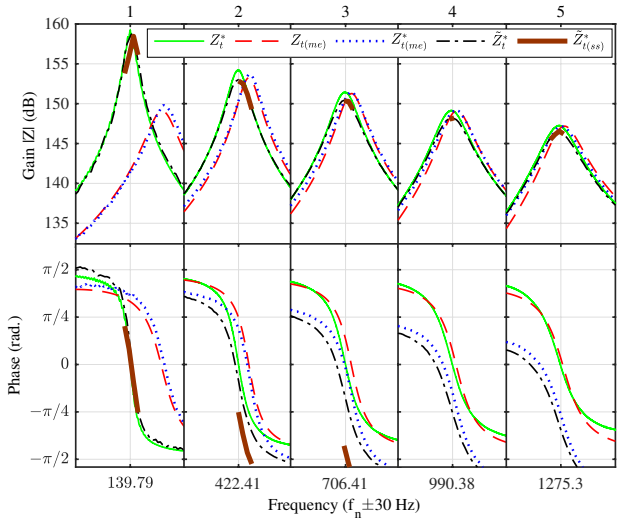

Figure 9: Originally measured, analytic coupled, measured coupled and measured uncoupled tube impedance curves ±30 Hz around the five first modes. The latter is also shown for a measurement using self-sustained oscillation signals ($\tilde{Z}^*_{t(ss)}$) (instead of a sine sweep used for the other measurements). Note that the phase of the fourth and fifth modes of $\tilde{Z}^*_{t(ss)}$ falls below $-\pi/2$. .

$Z_{t(me)}$, as theoretically calculated using equation (7) (represented in dashed red). A modal calculation using the coupled tube parameters $a_{n(me)}$ and $Q_{n(me)}$ in equation (4) resulted in a close match (not plotted). It can be seen that the modes of $Z_{t(me)}$ lying near to the loudspeaker's resonance are shifted upwards in frequency in comparison with Z^*_t. At higher frequencies, both the amplitude and phase are in much closer agreement.

Figure 9 also shows an impedance measurement of the loudspeaker-coupled tube: $Z^*_{t(me)}$ (in dotted blue), which was measured by applying the feedforward filter but not the feedback filter. The curves are close to the analytically calculated equivalent $Z_{t(me)}$, which also emphasises that the lead-lag compensator satisfactorily corrects the amplitude and phase response. The increasing phase shift at higher frequencies is explained by the phase-lag problem discussed in appendix B.

Furthermore, the addition of the feedback filter results in the impedance measurement $\widetilde{Z}^*_t$, which is also depicted in figure 9 (in black dash-dotted). The same deviations as were observed for the measured $Z^*_{t(me)}$ are still visible, but the result is fairly close to the original measured tube impedance Z^*_t. The zero-crossings, which are an important indicator for potential self-sustained playing frequencies, are reasonably close to the original resonance frequencies.

However, when the tube's input impedance is obtained from the self-sustained signals that appear during hybrid operation: $\widetilde{Z}^*_{t(ss)} = P_{ss}/Q_{ss}$ (the solid thick brown curve in figure 9), an important phase lag is noted, which increases with frequency. This could be a result of the synchronously phased harmonics, a signature of the air flow signal of a self-sustained wind instrument, which demands substantial physical effort from the actuator. It may be assumed that the loudspeaker mechanics include nonlinearities such as hysteresis which introduce this phase lag. Nevertheless, it should be mentioned that the phases of $\widetilde{Z}^*_t$ and $\widetilde{Z}^*_{t(ss)}$ coincide at the fundamental frequency, which ensures that higher notes can be still played, and have a reasonable pitch relation to the acoustic instrument.

4.4 Computing system

The hybrid operation requires a "real-time" feedback-loop that includes a numerical interface. The solution chosen for the prototype hybrid instrument described here involves the recompilation of a Linux kernel on standard PC architecture, which is covered by the *Xenomai* framework [23]. This system includes special drivers (by the *Analogy* software), which enable uninterrupted access to a *National Instruments* 6052E 16-bit acquisition card that provides analogue inputs and outputs. That is to say, when a program is compiled from C-code that includes specific *Xenomai* and *Analogy* driver-code, its execution gains full priority over all processes; this is also referred to as a "hard real-time" process.

In order to introduce these specific commands in the C-code that is generated from a Simulink program, we rely on the work by Benacchio et al., who created a patch-file that makes the necessary modifications to the C-code [24].

In this way, the system can be used with a minimum sampling time (without overruns) of $T = 25\,\mu s$, corresponding to a sampling rate of f_s =40 kHz (sufficient for capturing the frequencies produced by the instrument).

The analogue inputs are sampled with an analogue-to-digital (A/D) converter while calculated digital output data is simultaneously sent to the digital-to-analogue (D/A) converter (shown in the global block diagram in figure 3). In this process, some signal transformations occur. While the A/D converter contains an anti-aliasing low-pass filter and introduces quantisation noise, the D/A converter also involves a low-pass "reconstruction filter". However, given that a high sampling rate and bit depth are used, the effect of these transformations is negligible for the frequency and amplitude range of interest in this study. For the current system, as there are no sources of latency other than the A/D and D/A conversion itself, the total latency is restricted to a single sample only, so that the entire computing system's response, modelled by z^{-1}, can be neglected in this study.

5 Results

As the tube impedance $\widetilde{Z}_t$ is the ratio of pressure P and flow rate $\widetilde{Q}$, both of which are monitored and controlled by the computer, it is possible to use any excitation model to produce hybrid self-sustained sounds.

In this investigation, the single-reed mouthpiece model discussed in subsection 2.1 is chosen as the excitation model. The dynamic parameters (of importance to the brightness and in selecting the desired register) are held fixed to the values used in [25]: $\omega_r = 2\pi \times 2500\,\mathrm{rad\,s^{-1}}$ and $Q_r = 5$, which makes the reed operation close to quasistatic. Meanwhile the embouchure parameter ζ is varied over a range of values typical of those quoted in the literature for clarinets ($0.1 \lesssim \zeta \lesssim 0.4$) [16], while the dimensionless mouth pressure γ is varied from 0 to the point of extinction.

To evaluate the hybrid self-sustained operation, the previously described loudspeaker-resonator system was combined with the computing system (which applied the loudspeaker-compensating filters and the mouthpiece model). In this section, the hybrid results are compared with simulations of the entire instrument. In these simulations, the single-reed model is combined with the modal approximation of the tube (as described in section 2.2). This resonator model is numerically calculated with a fourth order Runge-Kutta solver applied on a series of 14 bandpass filters, which correspond to the second order transfer functions in equation (4).

Given that the deviation between the resonator simulation and the real resonator input impedance (see B.2.3) is much smaller than the uncompensated deviations introduced by the transducers for the case of the real hybrid instrument, the entire instrument simulations can be considered representative of an ideal hybrid instrument's functioning.

An important focus is the sound perceived by a listener. Therefore, a signal related to the pressure waves radiated by the instrument is calculated. A simplified, yet sufficiently relevant, "monopole" radiation model describes the temporal derivative of the pressure waves propagating downstream from the resonator (see e.g. [26]). It can be verified that this downstream (dimensionless) pressure corresponds to $(\bar{p}+\bar{q})/2$, so that the approximated external pressure can be written as:

$$\bar{p}_{ext} \propto \frac{d(\bar{p}+\bar{q})}{dt}. \tag{16}$$

In order to reduce the amplification of high frequency noise, prior to calculating the derivative, a steep (IIR, 33^{rd} order Butterworth) low-pass filter is applied, with a cut-off frequency of 4 kHz, just above the resonance frequency of the upper simulated mode.

To allow for a quantitative and useful comparison of hybrid and simulated sounds, so called "sound descriptors" are employed. These represent a standardised set of features that describe relational values derived from the spectral, temporal and harmonic representations of the sound. Sound descriptors can be meaningful characteristic features regarding both perception (to quantify the timbre mostly) and the instrument's acoustic functioning.

For the selection of useful descriptors, we rely on the work of Barthet, who extensively studied the timbre of the clarinet and its relation to the instrument's input parameters [27, 28]. His work resulted in the abstraction of a clarinet-related three-dimensional perceptive timbre space, based on the classification of a set of clarinet-synthesised sounds (using a realistic temporal mouth pressure envelope) by listeners. Then, an algorithmic procedure allowed for the correlation between these dimensions and the sound descriptors. For the current study, a number of highly correlated descriptors that are also of perceptual relevance have been adopted: the "Logarithmic Attack Time" (LAT), the "Spectral Centroid" (SC), and the "Odd/Even harmonics Ratio" (OER).

The LAT descriptor represents the logarithm (at a decimal base) of the time taken for the amplitude envelope to increase from 10% to 80% of the maximum amplitude value for the sound event. The SC represents the frequency of the centre of the spectrum, using the amplitude weight of each frequency, and has a robust connection with the perceived impression of "brightness". The OER is calculated as the ratio of odd and even harmonic amplitude components[2]. While the cylindrical closed-open resonator promotes a frequency spectrum dominated by odd harmonics, the mouthpiece model can also introduce even frequency components, which is the motivation behind the examination of this descriptor.

In addition, the fundamental frequency (f_0) and the mean (RMS) pressure evolution are studied. Given the known typical progression of the RMS mouthpiece pressure as a function of the mouth pressure progression [29], the RMS of $\bar{p}$ is calculated rather than $\bar{p}_{ext}$. Furthermore, the end of the attack time (EAT) is reported, which is the time when the amplitude envelope reaches 80% of its maximum, relative to the start of blowing. In contrast to the LAT, this time span expresses the delay between the mouth pressure onset and the resulting sound onset, which is an important aspect with respect to the timing of played notes.

Precise mathematical definitions of all these descriptors can be found in [27, 30]. The calculation of the descriptors is carried out using the MATIMBRE toolbox, a MATLAB program developed by Barthet [27, 28].

[2]The OER descriptor relies on a number of harmonic peaks in the spectrum. Here this number was set to 20 (both odd and even) harmonics, as above this value wrong peaks were sometimes identified.

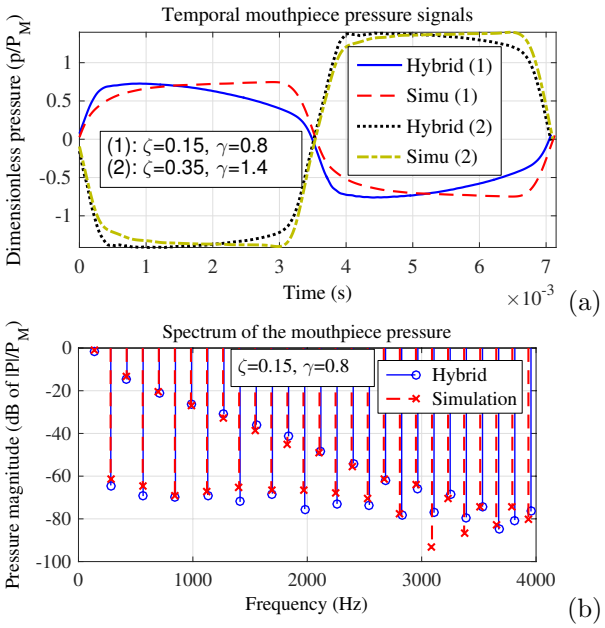

Figure 10: Temporal steady state mouthpiece pressure wave cycles for 2 input parameter states (a) and the Fourier series corresponding to the pressure wave cycle of the first state (b); both for the hybrid and simulated instruments.

5.1 Sustained sounds

As the resonator simulation is limited to 14 modes, only that part of the spectrum is considered, i.e. up to 3900 Hz.

Figure 10 (a) shows the temporal pressure waves produced by the hybrid and simulated instruments for two arbitrary constant input parameter states: $\{\zeta = 0.15, \gamma = 0.8\}$ and $\{\zeta = 0.35, \gamma = 1.4\}$. It can be seen that the amplitudes and wavelengths are closely matching and that the wave shapes are also in reasonable correspondence. Figure 10 (b) shows the Fourier series corresponding to the pressure wave cycles of the first mentioned parameter state. A very good overall match is achieved, particularly for the odd harmonics whose amplitudes differ by no more than 3 dB up to 3.5 kHz, while the first ten even harmonics resulting from the simulation are on average 3 dB louder. This level of agreement is obtained for all sounds within a parameter range that ensures a stable output (hereafter referred to as the "stable parameter range"), i.e. $\gamma < \frac{3}{4}\gamma_{ex}$ (with γ_{ex} the extinction threshold) and $\zeta \geq 0.1$, where the steady oscillation state is not easily influenced by other parameters such as noise, the imperfect loudspeaker and its model.

The dimensionless mouth pressure γ was varied from 0.33 to 2.2 for six values of ζ (between 0.1 and 0.35). The resulting internal ($\bar{p}$) and external ($\bar{p}_{ext}$) pressure signals for both the hybrid and simulated instruments were recorded and first judged by ear (the sounds can be downloaded here: `https://doi.org/10.21954/ou.rd.3848415.v1`). It is immediately apparent that it is difficult to aurally distinguish the hybrid and simulated results (the only noticeable difference being the higher noise level of the hybrid sounds, caused by the derivative in (16)).

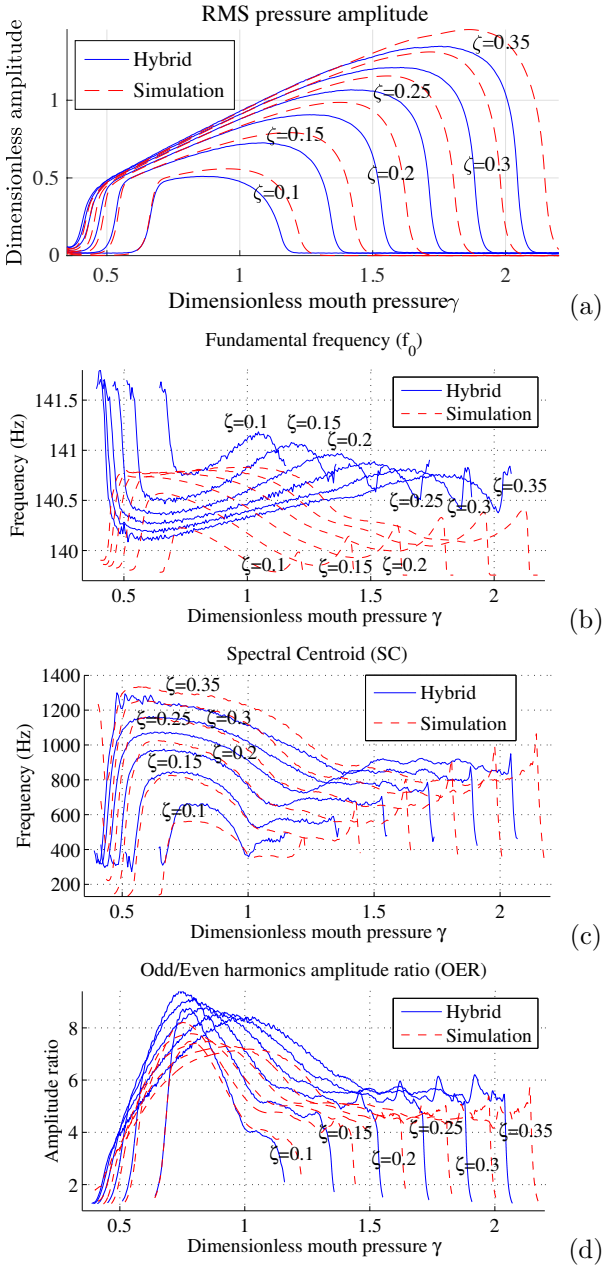

Figure 11: RMS pressure amplitudes (a), fundamental frequencies (b), Spectral Centroids (c) and Odd/Even ratios (d) of sounds produced by the hybrid and simulated instruments for various ζ and increasing γ values.

Figure 11 shows the evolution of the sound descriptors with increasing mouth pressure γ for the six values of ζ.

The hybrid and simulated RMS evolutions and extinctions in 11 (a) are in good agreement in the stable parameter range and also match to findings in the literature [29]. Even the oscillation thresholds, which are easily perturbed by noise, correspond closely. Above each oscillation threshold, the RMS of the hybrid results is lower than that of the sim-

ulations and extinction is reached at a lower mouth pressure. This could be explained by the fact that uncompensated loudspeaker effects (e.g. introducing the increasing phase lag noted in figure 9) can be interpreted as an increase in losses in the hybrid system.

For the fundamental frequency evolutions shown in 11 (b) there is less agreement between the hybrid and simulated sounds, however all variations are small (<1.5 Hz or <18 cent) and are almost imperceptible.

The frequency variation can be explained by the well known theory that for an inharmonic resonator (where the resonance frequencies are not integer multiples of the first resonance frequency), the playing frequency changes with the brightness of the sound (see e.g. [31]). This can be understood from the fact that the first few resonator modes are known to maintain the self-sustained oscillation [32]; and hence, the preferred oscillation frequency results from a weighting of these modes by the spectrum of the mouthpiece pressure. As can be seen from the first five modes of Z_t^* in figure 9, the tube has a positive inharmonicity (i.e. the resonance frequencies shift upwards with increasing frequency, e.g. 1275.3 Hz/9 =141.7 Hz > 139.79 Hz), which explains the positive correlation between the fundamental frequency and Spectral Centroid curves resulting from the simulations (shown in 11 (c)). On the other hand, the observed phase decrease due to uncompensated nonlinear loudspeaker effects in $\widetilde{Z}_{t(ss)}$ in figure 9, indicates that during hybrid self-sustained operation, the resonator is perceived as negatively inharmonic. This explains the inverse correlation between the fundamental frequency and Spectral Centroid curves resulting from the hybrid operation.

Another discrepancy concerns the initial difference in fundamental frequency. The simulation starts at a fundamental frequency close to the first modal frequency of 139.8 Hz (which is to be expected, as the oscillation is still close to sinusoidal and as such, relies almost solely on this mode with an almost quasistatic reed). However, the fundamental frequency of the hybrid instrument starts a few Hz above 139.8 Hz (the temperature used in the simulation matched that observed during the operation of the hybrid instrument). A possible reason for this initial pitch shift might be an imperfect compensation by the loudspeaker-correcting filter $\widetilde{H}_{LS}^{-1}$ which would introduce a slight phase shift for the first mode and as such a shift of the frequency at which instability occurs. This can be verified from figure 9, where the phase response of the first mode of $\widetilde{Z}_t^*$ is indeed slightly right-shifted from Z_t^* (by approximately 1 Hz, found by zooming).

It should be noted that higher modes, which don't maintain the self-sustained operation, still filter the high frequency spectrum of the sound. This, in combination with the f_0 variation, in turn also causes slight variations of other descriptors, such as the Spectral Centroid.

For $\zeta = 0.15$ and $\zeta = 0.2$ the simulated and hybrid Spectral Centroid curves in 11 (c) are very well-correlated in the stable parameter range. Higher ζ values (producing a richer sound) seem to increase the SC of the simulated sounds slightly more. This can be partly explained in terms of the previously discussed difference in fundamental frequency. Provided the embouchure parameters remain unchanged, a higher fundamental frequency will lead the higher harmonics towards the tube's resonant peaks so that the SC increases. This is confirmed by the differences between the hybrid and simulated results in terms of both fundamental frequency and Spectral Centroid. Nevertheless, the differences are relatively small and all progressions are similarly rapidly increasing after the note appearance, to then decrease until its extinction.

The Odd/Even Ratio curves in 11 (d) show that the simulation generally produces sounds with more even harmonics than the hybrid instrument does, which was also observed in the spectra of figure 10 (b). A possible explanation might be less well approximated anti-resonances in Z_t (given that this impedance is composed of filters that imitate the resonances only). However, it must be noted that the presence of even harmonics is almost entirely accredited to the flow rate component $\bar{q}$ in equation (16). But again, the difference is relatively small and both curve sets follow a similarly shaped evolution, with a maximum peak occuring approximately a third of the distance between the oscillation threshold and the extinction threshold (with maxima for $\zeta = 0.15$ to $\zeta = 0.25$), and rapidly decreasing before and after that mouth pressure.

These findings are all in broad agreement with those of Almeida et al. [33], who excited a real clarinet using a basic artificial mouth and then took a similar evaluation approach to that used in this study. However, the level of the agreement with Almeida's results is much smaller than the correlation between the hybrid and simulated results reported here. Hence, the similarity between Almeida's evaluation of a real clarinet and the results presented in the current paper only indicates that the single-reed model employed in this study reflects the behaviour of a real clarinet mouthpiece, played by an artificial mouth.

Nevertheless, it should be noted that the comparison of real and hybrid instruments could be particularly useful to study self-sustained operations in more complex resonators, and notably during fingering transitions, as these are difficult to simulate. This is also stressed in another paper by Almeida [12].

5.2 Attack sounds

While clarinet players mostly initiate a note by tonguing, it is known that the tongue action mainly determines the timing of the initial transients [34] rather

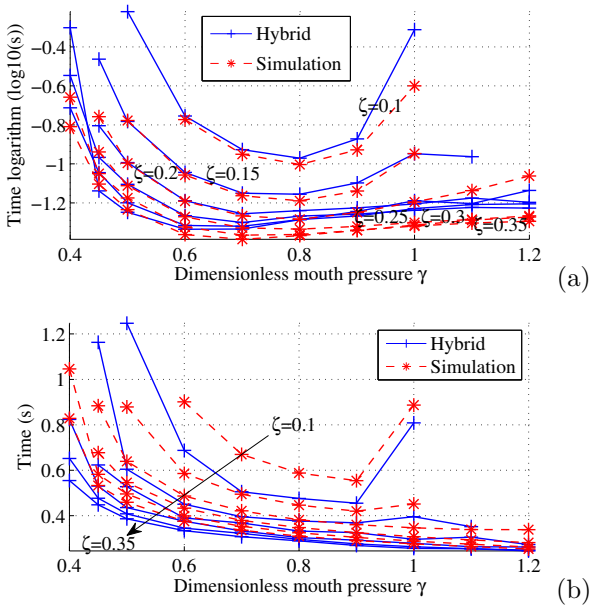

Figure 12: Logarithmic Attack Times (a) and End of Attack Time (b) of sounds produced by the hybrid and simulated instruments for various static input parameters.

than the attack time of the note onset. Hence, while the applied single-reed model doesn't include the effect of the tongue, it is sufficient to apply a steep increase of the mouth pressure to imitate a tongue release.

Using the same six ζ values, ten constant γ values between 0.4 and 1.2 were evaluated and the attack time (i.e. the time required for the oscillation to settle to the steady state regime) measured. To best match real playing conditions, the mouth pressure was gradually introduced. However, so as not to influence the attack time, the rise time (to reach γ from 0) must be shorter than the attack time. For the particular set of ζ values, a rise time of 0.3 s appeared to be sufficient (shorter rise times did not influence the resulting attack time). Figure 12 (a) shows the resulting Logarithmic Attack Times while figure 12 (b) shows the End of the Attack Times, for both hybrid and simulated instruments.

While the hybrid and simulated LAT results are in very good agreement over a large range of input parameters, the actual sound onsets, indicated by the EAT results, show important deviations, in particular for low γ values. The additional delay in the simulations may be due to the absence of irregularities that may help stimulate the attack, such as noise (present in real wind instruments, due to the flow turbulence). This hypothesis is supported by the findings of an additional experiment: a repeated simulation with an added noise signal (of similar amplitude to the noise present with the hybrid instrument) resulted in a reduction of up to 30% in the EAT compared with the noiseless simulations. Given the importance of timing, this aspect might be of consideration for reed instrument physical models. (The added noise did not significantly influence the LAT descriptor.)

During transients in a real instrument, the mean volume flow changes at a frequency that lies far below the loudspeaker resonance frequency. Given that the hybrid instrument filters out this part of the spectrum (with no DC flow generated by the loudspeaker), the transients will not be perfectly reproduced, which might explain certain small audible differences in the attack sounds for a few specific mouthpiece parameters.

Also these findings on attack transients are in good qualitative agreement with a recent study on the transients in a real clarinet (played with an artificial mouth). This study was conducted by Li et al. [34], following a similar approach as Almeida [33]. However, as with the sustained sounds, the agreement between our and their findings is much smaller than the observed correlation between the simulated and hybrid results.

5.3 Overall comments

For both sustained and attack sounds, over most of the stable parameter range, the difference for each descriptor curve between the simulated and the hybrid results is less than 5%. However, this deviation is exceeded when the extinction threshold is approached, as the sound changes rapidly towards this threshold and the threshold value itself appears to decrease with the noisiness of the sound. The increased noisiness in the measurements obtained with the hybrid instrument decreased the thresholds by about 8%.

It should also be noted that a generally excellent repeatability is found with the hybrid instrument (which is why no error bars are used). However, the imperfect timing precision of the real-time computing system introduces a slight jitter (manifested as an additional noise signal) whose mean time deviation (around $\pm 3\,\mu$s) is found to change over longer periods (hours or days). This slow irregular fluctuation is manifested as a long-term non-repeatability of the hybrid sounds.

The reported experiments were all carried out with the P_M parameter set at 100 Pa, but linearly proportional hybrid signals were obtained for P_M values ranging from 12 Pa to 300 Pa. However, this range lies well below the beating pressures found in real clarinets, which tend to range from $P_M = 4$ kPa to 10 kPa [35]. Consequently, the current hybrid instrument prototype cannot be used to investigate the nonlinear sound propagation within the resonator that can occur at large amplitudes in real wind instruments.

6 Concluding remarks

A hybrid wind instrument with a loudspeaker as the flow actuator has been successfully developed, in-

formed by a quantitative study of the component parts and their interaction. This in turn informed the design of two filter chains: a feedback filter to compensate for the coupled interaction between the loudspeaker and resonator, and a feedforward filter to correct for the (not initially flat) loudspeaker response. A number of measurements have been carried out to derive the filter parameters and to verify their importance.

The performance of the prototype instrument has been assessed via comparison with simulations, demonstrating the successful implementation of the hybrid system. The hybrid and simulated descriptor curves are generally in good agreement. In particular, they show similar progressions, indicating that the mouth control techniques maintain their effect, and characteristic values such as the beating pressure and the oscillation thresholds are approximately the same in both the hybrid and simulated curves.

The successful development of the hybrid instrument can also be assessed by considering it in relation to a real wind instrument. To this end, the prototype system has been empirically tested by connecting it to a real clarinet resonator, resulting in more realistic clarinet sounds than achieved with the cylindrical tube resonator (see `http://dx.doi.org/10.21954/ou.rd.3848115` for a video of this, where it can be seen and heard that a note-range of 2 octaves is covered and that the notes all sound reasonably similar in timbre).

To further develop the hybrid instrument, the question of whether the absence of the mean air flow through the instrument adversely affects the sound produced could be investigated. This could be addressed by, for example, injecting a separate mean flow component via a capillary tube connected to the entrance of the instrument.

In addition, the mouthpiece model used in this study is relatively basic and further refinements could be introduced. For example, the flow that is induced by the reed movement could be included [32], and the introduction of a gradually increasing reed stiffness would better represent the curvature of the mouthpiece tip [36]. As well as better matching the real physical situation, such additional inclusions might lead to a calculated flow signal that can be better realised by the loudspeaker (given that the current model leads to discontinuous reed beating which imposes abrupt flow variations).

Another area for further development is in relation to the dynamic range of the hybrid instrument, independent of any spectral variation. For the case of a resonator with a linear acoustic response (which is assumed in the simulations), varying P_M would only change the amplitude of the sound produced. However, the hybrid instrument's dynamic range is limited by noise and saturation thresholds introduced by the equipment. It is found that below $P_M = 12\,\mathrm{Pa}$, noise starts to dominate in the sound produced by the prototype hybrid instrument. Meanwhile, above $P_M = 300\,\mathrm{Pa}$, loud and spectrally rich sounds (i.e. with high SC and RMS values) start to become saturated. A more powerful prototype could involve a redesign of the loudspeaker so that the required added membrane mass is achieved by additional coil weight.

Another limitation of the current prototype is the restricted input parameter range. For dimensionless mouth pressure values lying in the range $0.4 < \gamma < 0.6$, an unstable oscillation appears when the mouthpiece parameter is increased above $\zeta = 0.35$, leading to the timbre produced deviating from the expected clarinet sound. Such a timbral deviation is not observed in either the simulations or in a real instrument.

A further future development of the hybrid instrument prototype concerns the exploration of other excitation models. Physical models that are closely related to the currently used single-reed model (such as double-reed [37] and lip-reed models) are easy to implement. Moreover, to fully exploit the musical potential of the hybrid approach, non-wind excitation models such as the bow-string interaction mechanism [38], or models that are not necessarily related to any physical reality, could be combined with an acoustic resonator using the prototype set-up. However, each model requires discretisation, which is not always straightforward.

Finally, for a hybrid instrument to be fully utilised in musical performance, it is important to maximise the expressive control possibilities available to a musician. As the hands are already occupied in applying different fingerings to the resonator, a mouth controller capturing mouth and lip pressure signals could be introduced to the hybrid set-up. In addition, sensors to detect instrument position, and accelerometers to measure the motion of the instrument body could be incorporated.

Acknowledgements

Special thanks goes to Simon Benacchio and his team at IRCAM, who devoted their time, effort and space to help setting up the real-time computer, and to Mathieu Barthet, who provided his MATIMBRE toolbox for the sound descriptor calculations.

The authors would also like to thank the anonymous reviewers for their valuable comments and suggestions to improve the quality of the paper.

References

[1] J. Guérard and X. Boutillon. Real-time wave separation in a cylindrical pipe with applications to reflectometry, echo-cancellation, and a hybrid

musical instrument. In *Proc. 16th ICA 98*, number 1, pages 2261–2262, 1998.

[2] J. Guérard. *Modélisation numérique et simulation expérimentale de systèmes acoustiques - Application aux instruments de musique*. PhD thesis, Université Pierre et Marie Curie - Paris VI, 1998.

[3] P.B. Pickett and W.R. Saunders. *An Investigation of Active Tonal Spectrum Control as Applied to the Modern Trumpet*. PhD thesis, Virginia Polytechnic Institute and State University, 1998.

[4] H. Boutin. *Méthodes de contrôle actif d'instruments de musique. Cas de la lame de xylophone et du violon*. PhD thesis, Université Pierre et Marie Curie, 2011.

[5] E. Berdahl. *Applications of Feedback Control to Musical Instrument Design*. PhD thesis, Stanford University (CCRMA), Stanford University, 2009.

[6] T. Meurisse, A. Mamou-Mani, R. Caussé, B. Sluchin, and D. Sharp. An active mute for the trombone. *J Acoust Soc Am.*, 2016.

[7] S. Benacchio, B. Chomette, A. Mamou-Mani, and F. Ollivier. Modal PD state active control applied to a simplified string instrument. *J. Vib. Control*, 2016.

[8] G. Weinreich and R. Caussé. Digital and analog bows: Hybrid mechanical-electrical systems. In *ICASSP*, pages 1297–1299, 1986.

[9] C. Maganza. *Excitations non linéaire d'un conduit acoustique cylindrique. Observations de doublements de période précédant un comportant chaotique. Application à la Clarinette*. PhD thesis, Université du Maine, 1985.

[10] N. Grand. *Etude du seuil d'oscillation des systèmes acoustiques non-linéaires de type instrument à vent*. PhD thesis, Université Paris 7, 1994.

[11] K. Buys and C. Vergez. A hybrid reed instrument: an acoustical resonator with a numerically simulated mouthpiece. In *Proc. Acoust. 2012*, Nantes, 2012.

[12] A. Almeida, M. Laruaz, and J.-P. Dalmont. Attack transients in a loudspeaker / resonator coupled system. In *Proc. 20th Int. Congr. Acoust. ICA 2010*, number August, pages 1–4, 2010.

[13] A. Hirschberg. Aero-acoustics of wind instruments. In A. Hirschberg, J. Kergomard, and G. Weinreich, editors, *Mech. Music. Instruments*. Springer, Wien, 1995.

[14] T.A. Wilson and G.S. Beavers. Operating modes of the clarinet. *J. Acoust. Soc. Am.*, 56:653–658, 1974.

[15] D. Ferrand and C. Vergez. Blowing machine for wind musical instrument : toward a real-time control of the blowing pressure. *2008 16th Mediterr. Conf. Control Autom.*, 2008.

[16] A. Chaigne and J. Kergomard. *Acoustique des instruments de musique*. Belin, 2008.

[17] F. Silva, J. Kergomard, C. Vergez, and J. Gilbert. Interaction of reed and acoustic resonator in clarinetlike systems. *J. Acoust. Soc. Am.*, 124(5):3284–3295, 2008.

[18] R.H. Small. Direct Radiator Loudspeaker System Analysis. *J. Audio Eng. Soc*, 20(5):383–395, 1972.

[19] L.L. Beranek. *Acoustics*. McGraw-Hill electrical and electronic engineering series. McGraw-Hill, 1954.

[20] A.D. Pierce. *Acoustics: An Introduction to Its Physical Principles and Applications*. Acoustical Society of America, 1989.

[21] W.C. Messner, M.D. Bedillion, L. Xia, and D.C. Karns. Lead and lag compensators with complex poles and zeros: Design formulas for modeling and loop shaping. *IEEE Control Syst. Mag.*, 27(February):44–54, 2007.

[22] P.J. Chapman. Thermal simulation of loudspeakers. *Audio Eng. Soc. Conv. 104*, 1998.

[23] Xenomai: Real-Time Framework for Linux. `http://www.xenomai.org`.

[24] S. Benacchio, R. Piéchaud, and A. Mamou-Mani. Active Control of String Instruments using Xenomai. In *15th Real Time Linux Work.*, 2013.

[25] P. Guillemain, J. Kergomard, and T. Voinier. Real-time synthesis of clarinet-like instruments using digital impedance models. *J. Acoust. Soc. Am.*, 118(1):483–494, 2005.

[26] F. Jacobsen. Propagation of sound waves in ducts. *Lect. notes*, (31260), 2011.

[27] M. Barthet, P. Guillemain, R. Kronland-Martinet, and S. Ystad. From Clarinet Control to Timbre Perception. *Acta Acust united Ac*, 96(4):678–689, jul 2010.

[28] M. Barthet. *De l'interprète à l'auditeur: une analyse acoustique et perceptive du timbre musical*. PhD thesis, Université de la Méditerranée Aix-Marseille II, 2009.

[29] M. Atig, J.-P. Dalmont, and J. Gilbert. Saturation mechanism in clarinet-like instruments, the effect of the localised non-linear losses. *Appl. Acoust.*, 65(12):1133–1154, dec 2004.

[30] G. Peeters, B.L. Giordano, P. Susini, N. Misdariis, and S. McAdams. The Timbre Toolbox: Extracting audio descriptors from musical signals. *J. Acoust. Soc. Amer.*, 130(5):2902–2916, nov 2011.

[31] A.H. Benade. *Fundamentals of Musical Acoustics*. Courier Dover Publications, second edition, 1990.

[32] J.-P. Dalmont, B. Gazengel, J. Gilbert, and J. Kergomard. Some aspects of tuning and clean intonation in reed instruments. *Appl. Acoust.*, 46(1):19–60, jan 1995.

[33] A. Almeida, D. George, J. Smith, and J. Wolfe. The clarinet: how blowing pressure, lip force, lip position and reed "hardness" affect pitch, sound level, and spectrum. *J. Acoust. Soc. Am.*, 134(3):2247–55, sep 2013.

[34] W. Li, A. Almeida, J. Smith, and J. Wolfe. The effect of blowing pressure, lip force and tonguing on transients: A study using a clarinet-playing machine. *J. Acoust. Soc. Am.*, 140(2):1089–1100, 2016.

[35] J.-P. Dalmont, J. Gilbert, and S. Ollivier. Nonlinear characteristics of single-reed instruments: Quasistatic volume flow and reed opening measurements. *J. Acoust. Soc. Am.*, 114(4):2253–2262, 2003.

[36] F. Avanzini and M. Van Walstijn. Modelling the mechanical response of the Reed-mouthpiece-lip system of a clarinet. Part I. A one-dimensional distributed model. *Acta Acust united Ac*, 90(3):537–547, 2004.

[37] P. Guillemain. A digital synthesis model of double-reed wind instruments. *EURASIP J. Appl. Signal Processing*, 2004(ii):990–1000, 2004.

[38] M.E. McIntyre, R.T. Schumacher, and J. Woodhouse. On the oscillations of musical instruments. *J. Acoust. Soc. Amer.*, 74(5):1325–1345, 1983.

[39] W. Klippel and U. Seidel. Fast and accurate measurement of linear transducer parameters. *Prepr. Eng. Soc.*, pages 1–7, 2001.

[40] J. Blauert and P. Laws. Group delay distortions in electroacoustical systems. *J. Acoust. Soc. Am.*, 63(5):1478–1483, 1978.

[41] D. Sharp, A. Mamou-Mani, and M. Van Walstijn. A Single Microphone Capillary-Based System for Measuring the Complex Input Impedance of Musical Wind Instruments. *Acta Acust united Ac*, 97(5):819–829, sep 2011.

A Discretisations

A.1 Single-reed model

A discretisation of the single-reed model presented in subsection 2.1 is developed here. The subscript n is used to designate the sample number in discrete time. The discretisation steps are briefly summarised here (a detailed development can be found in [25]).

The reed's dynamics can be exactly discretised using classical central numerical differentiation schemes that only rely on previous samples, so that:

$$\bar{y}_n = \frac{\bar{\Delta p}_{n-1} + (\frac{f_s^2}{\omega_r^2} - 1)\bar{y}_{n-1} + (\frac{f_s}{2Q_r\omega_r} - \frac{f_s^2}{\omega_r^2})\bar{y}_{n-2}}{\frac{f_s^2}{\omega_r^2} + \frac{f_s}{2Q_r\omega_r}}, \tag{17}$$

with $f_s = \frac{1}{T}$ the sampling rate. By decomposing the dimensionless mouthpiece pressure into a component $\bar{q}$ resulting from the entering flow rate and a pressure $\bar{p}_h$ arising from the upstream and reflected pressure wave in the resonator: $\bar{p}_n = \bar{q}_n + \bar{p}_{h,n}$, the explicit equation can be found:

$$\bar{q}_n = \frac{1}{2}\operatorname{sgn}(\gamma - \bar{p}_{h,n})\bar{S}_{f,n}^2\left(\sqrt{1 + \frac{4|\gamma_n - \bar{p}_{h,n}|}{\bar{S}_{f,n}^2}} - 1\right), \tag{18}$$

with $\bar{S}_{f,n} = \zeta_n\mathcal{H}(\bar{y}_n + 1)(\bar{y}_n + 1)$, the dimensionless reed opening area at time instance n.

This equation does not depend on $\bar{q}_n$, but $\bar{p}_{h,n}$ is required, which can be obtained from the upstream pressure at the resonator entrance. While for the case of numerically simulated resonators, that value is retrievable, in a hybrid instrument latency is involved, so that a theoretically relevant hybrid instrument implementation can be built with an additional microphone a distance Tc from the resonator entrance. However with a single microphone, $\bar{p}_{h,n-1}(= \bar{p}_{n-1} - \bar{q}_{n-1})$ can be used in place of $\bar{p}_{h,n}$. This approximation only introduces a minor delay, which only becomes of importance at high frequencies. Given that the high frequency content of $\bar{p}_h$ is low (as higher frequencies are only poorly reflected at the open end of the resonator), the approximation error and the chance for undesirable instabilities is small.

A.2 Loudspeaker correction filter

For numerical simulation, the derivative term of the continuous time loudspeaker correction filter expression (12) can be approximated by a discrete transfer function, using the "Euler backward method" (providing a causal first order "Finite Difference Approx-

imation"):

$$M_m\ s \approx \frac{M_m\ (z-1)}{T\ z}, \tag{19}$$

with T, the sample time. While this discretisation introduces an extra group delay of half a sample, the scheme ensures a causal and stable implementation with largely sufficient precision.

The Euler backward scheme also results in a well-approximated digital equivalent of the lead-lag filter (whose continuous time expression is given by equation (14)), given that its poles and zeros are small:

$$H_{LL}(z) = H_{LL}(s \to \frac{z-1}{T\ z}). \tag{20}$$

B Measurement of loudspeaker and tube parameters

To identify all parameters of the coupled loudspeaker-tube system a method related to the one proposed by Klippel was selected [39]. However, whereas Klippel's method is designed for use on a standalone loudspeaker, the method proposed here was applied to the loudspeaker coupled to the tube. The proposed method involves two measurements and four least square linear regressions. The regressions were carried out on the frequency domain representations of the measured data and enabled retrieval of both the loudspeaker and resonator parameters.

For reference, all of the obtained loudspeaker parameters and lead-lag filter coefficients are shown in table 1 in the main body of this paper.

B.1 Measurement 1

For the first measurement, a resistor with resistance R_s was placed in series with the loudspeaker and a sine wave signal with an amplitude of 0.3 V was supplied, swept in frequency from 0 kHz to 1 kHz over 20 s. This amplitude is of the same order as the hybrid signals encountered in this study, and covers about half the loudspeaker's linear dynamic range. The voltages across both the resistor and the loudspeaker were measured so that the current (and thus the speaker's electrical input impedance) could be derived, as in equation (8). The loudspeaker's membrane velocity was measured synchronously using a laser-Doppler-vibrometer. The measured values were then inserted into the following two alternative expressions for the impedance:

$$Z^*_{e(mt)} = \frac{V^*}{I^*} \tag{21a}$$

$$Z^*_{e(mt)} = \frac{Z_e\ V^*}{V^* - Bl\ \dot{X}^*}, \tag{21b}$$

where the asterisks refer to measured quantities.

A regression using both expressions resulted in a good match (see figure 13) enabling the retrieval of precise electrical loudspeaker parameters Bl and R_e.

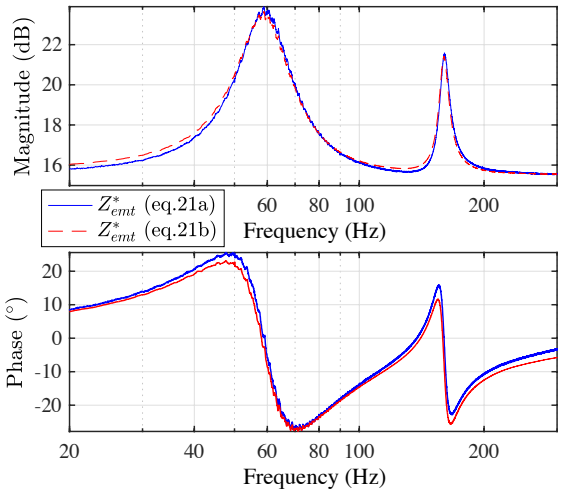

Figure 13: Regression of the electrical loudspeaker input impedance $Z^*_{e(mt)}$ using equations (21a) and (21b).

We note that the observed phase lag in the impedance obtained with equation (21b) increases with frequency and isn't taken into account by our model.

Contrary to what the loudspeaker model predicts, the measured input-to-output phase response increases more and more with frequency. While there is no mention of a group delay effect in the literature on loudspeaker modelling, this expression is more frequently used in literature focussed on perception. For instance Blauert states: "Common loudspeakers and earphones are not necessarily minimum-phase systems but show additional all-pass characteristics. The additional group delays caused by these characteristics are on the order of 400 µs" [40]. For comparison, the difference in the group delays derived from the phase responses of the input impedances Z^*_t and $\widetilde{Z}^*_{t(ss)}$ (which include the loudspeaker) in figure 9 are respectively 125 µs and 300 µs.

Given that the velocity measurement is used in equation (21b), the phase lag is reflected in the measurement with that equation. Hence, for a correct parameter estimation the regression is applied from 20 Hz to 300 Hz only.

B.2 Measurement 2

In the second measurement, the series resistance was left out so that the low amplifier output impedance and, consequently, the loudspeaker's Q_{ts}-factor were maintained. Here, the supplied sine wave signal was swept from 0 kHz to 5 kHz over 55 s for both a 0.3 V and a 0.6 V amplitude, in order to observe possible nonlinear effects. The amplifier's input voltage was captured, together with the membrane velocity and the pressure in front of it. The amplifier gain was

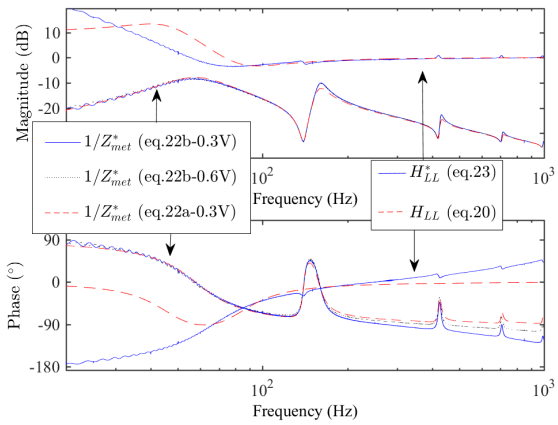

Figure 14: A regression of two mechanical loudspeaker reciprocal impedances $1/Z^*_{m(et)}$, obtained by equation (22a) (for a 0.3 V amplitude) and equation (22b) (for 0.3 V and 0.6 V amplitudes) and a regression of $\hat{Q}/Q^*$ with the H_{LL} compensator transfer function.

derived before the measurement, so that the voltage V delivered by the amplifier could be obtained.

B.2.1 Identifying loudspeaker mechanical parameters

The measurements were then inserted into equation (9), so that a regression with:

$$1/Z^*_{m(et)} = \frac{1}{Z_{m(e)} + S_d \, \frac{P^*}{\dot{X}^*}} \tag{22a}$$

$$1/Z^*_{m(et)} = \frac{Z_e \; \dot{X}^*}{V^* \; Bl}, \tag{22b}$$

using the expression for $Z_{m(e)}$ in (5), revealed all mechanical loudspeaker parameters (note that the inverse impedances are needed for optimal conversion).

The regressed curves (presented in figure 14) show a good correlation. At higher frequencies the same increasing phase lag behaviour is observed, but it is interesting to note that the measurement with the 0.6 V input signal is less affected.

B.2.2 Identifying lead-lag filter coefficients

The same measurement data can be used to find appropriate coefficients for the lead-lag compensator H_{LL}. The targeted range for this filter is between the loudspeaker resonance frequency and the frequency where the effect of the loudspeaker's damping and stiffness becomes negligible, i.e. 80 Hz to 300 Hz for our set-up.

Using the obtained electrical and mechanical loudspeaker parameters and the measured pressure signal P^*, the signal $\widehat{Q}^*$ can be derived by inversely applying the feedback and feedforward filters to the measured amplifier output voltage V^*. A regression using the lead-lag equation (20) was applied on the ratio between this input and output:

$$H^*_{LL}(f = [80, 300]) = \frac{\widehat{Q^*}}{S_d \; \dot{X}^*}, \tag{23}$$

which is also shown in figure 14, revealing an effective loudspeaker resonance compensation above $\omega_{LS} (= 2\pi \times 67.4 \, \mathrm{rad\,s^{-1}})$.

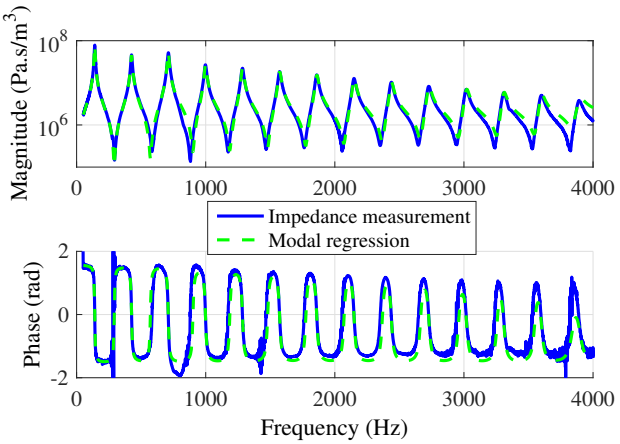

Figure 15: Fourteen first modes of the measured tube impedance Z^*_t (solid line) and its modal regression using equation (4) (dashed line).

B.2.3 Identifying modal tube coefficients

This measurement data and the S_d value (obtained via the first regression) also enabled the measurement of the input impedance of the resonator $Z^*_t = \frac{P^*}{\dot{X}^* S_d}$. Figure 15 shows the magnitude and phase of this impedance (solid line), along with a modal approximation (dashed line), which is derived from the measured impedance by regression, using equation (4) (thereby revealing the modal parameter values). The resonance frequencies of the regression are found with a ± 2 cent precision and, over a large range around the resonances, the magnitude does not deviate by more than ± 0.3 dB from the measurement.

This method is compared with other input impedance measurement techniques (e.g. the "capillary tube method" [41]) and is found to provide a measurement with the closest match to a theoretically obtained curve, except in terms of the phase at frequencies greater than 2 kHz, where the phase-lag issue arises (which is why the measurement with the 0.6 V signal is used here). Nevertheless, the regression can be focussed on the magnitude response for that frequency range, resulting in a corrected phase. Moreover, the phase response at such high frequencies doesn't affect self-sustained oscillations at the tube's first register note. As such, using a frequency range of 20 Hz to 4050 Hz, the parameters of 14 modes are identified.